

Cascaded Transfer: Learning Many Tasks under Budget Constraints

Eloi Campagne^{1,2} Yvenn Amara-Ouali^{2,3} Yannig Goude^{2,3} Mathilde Mougeot^{1,4} Argyris Kalogeratos¹

Abstract

Many-Task Learning refers to the setting where a large number of related tasks need to be learned, the exact relationships between tasks are not known. We introduce the *Cascaded Transfer Learning*, a novel many-task transfer learning paradigm where information (e.g. model parameters) cascades hierarchically through tasks that are learned by individual models of the same class, while respecting given budget constraints. The cascade is organized as a rooted tree that specifies the order in which tasks are learned and refined. We design a cascaded transfer mechanism deployed over a minimum spanning tree structure that connects the tasks according to a suitable distance measure, and allocates the available training budget along its branches. Experiments on synthetic and real many-task settings show that the resulting method enables more accurate and cost-effective adaptation across large task collections compared to alternative approaches.

1. Introduction

Modern learning systems increasingly operate in settings where a large number of related tasks must be handled under various constraints (e.g. data scarcity, computational power, fixed training budget). Such regimes arise naturally in personalized or localized applications, where each task is associated with only a small amount of data and independent training quickly becomes inefficient (Fallah et al., 2020). In these contexts, exploiting relationships across tasks is essential for building accurate models in frugal settings, as supported by both empirical and theoretical analyses in multi-task learning (Ciliberto et al., 2015).

Multi-Task Learning (MTL) has been developed to lever-

¹Centre Borelli, Université Paris-Saclay, CNRS, Ecole Normale Supérieure Paris-Saclay, France ²EDF R&D, Palaiseau, France

³Laboratoire de Mathématiques d'Orsay (LMO), Université Paris-Saclay, Faculté des Sciences d'Orsay, France ⁴ENSIIE, Évry-Courcouronnes, France. Correspondence to: Eloi Campagne and Argyris Kalogeratos <name.surname@ens-paris-saclay.fr>.

age shared information across tasks through joint training. Main approaches include feature-sharing architectures, low-rank parameterizations, and task clustering methods that explicitly model task relationships (Zhang & Yang, 2018; 2021; Ruiz et al., 2024). While effective, such methods require synchronized, globally coordinated optimization across tasks, leading to substantial memory or communication overhead. Moreover, MTL is highly sensitive to task relatedness (Standley et al., 2020), and inferring task relationships from data is often costly or assumption-heavy, motivating the use of *a priori* structures.

Many-Task Learning (MaTL) extends this setting to hundreds or thousands of tasks whose relatedness is only partially observable, often under strict resource constraints or at the cost of training very large models (Yu et al., 2024). Scaling to this regime typically requires mechanisms that control parameter sharing and interference, such as task-specific routing (Strezoski et al., 2019), hierarchical architectures (Hashimoto et al., 2017; Liu et al., 2021), or transferability-based task selection (Tan et al., 2024). Furthermore, recent studies on large-scale multi-task pre-training underscore the dualities of both the potential and the practical complexity of this regime (Aribandi et al., 2022). In particular, centralized joint optimization or training very large multi-task models quickly becomes computationally prohibitive and environmental costly. This phenomenon has been also documented in the context of federated optimization, where the conventional centralized assumptions become invalid at scale (Reddi et al., 2021). These limitations motivate the use of MaTL approaches, which rely on scalable, structured transfer mechanisms across tasks. These mechanisms explicitly account for locality, heterogeneity, and per-task budget constraints.

Transfer Learning (TL) naturally enters in the frame when thinking about sharing information from one task to another without global joint training. TL methods are commonly categorized as instance-based, feature-based, parameter-based, or relational (Pan & Yang, 2009; Weiss et al., 2016; Zhuang et al., 2020). In practice, TL is straightforward to deploy in modern neural settings and scales well to large numbers of downstream tasks, but it typically treats each source-target pair independently (Kornblith et al., 2019). As a result, large-scale TL systems often rely on simple star-shaped transfer schemes, where a single pretrained model is adapted sepa-

rately to many tasks (Raffel et al., 2020; Kolesnikov et al., 2020). Beyond such configurations, classical TL provides little guidance on how to organize or coordinate transfers across a large collection of tasks, limiting its applicability as a primary mechanism for structuring information flow in the MTL and, more critically, the MaTL regime.

Related applications. The MaTL regime appears naturally in personalized modeling, distributed sensing, and large-scale prediction settings, where scalable mechanisms are needed to exploit task relatedness across many heterogeneous tasks. Typical application domains include energy networks, transportation, and retail, in which thousands of related prediction problems arise in parallel (Laptev et al., 2018; He et al., 2019; Antoniadis et al., 2024). In many real-world deployments, tasks must be adapted locally with limited data and computational resources, such as spatially distributed prediction over large sensor networks, climate grids, or client-level personalization in federated systems. Representative examples include large-scale spatiotemporal forecasting benchmarks such as *SubseasonalClimateUSA* (Mouatadid et al., 2023) and *WeatherBench 2* (Rasp et al., 2024), which frame climate and weather prediction as collections of localized tasks evaluated under realistic computational constraints. Similar challenges arise in industrial hierarchical forecasting at scale in retail and energy systems (Sprangers et al., 2024), as well as in personalized federated learning, where each device constitutes a distinct task requiring local adaptation under heterogeneity, as exemplified by Ditto (Li et al., 2021).

Contributions. In this work, we focus on a frugal many-task setting in which each task is refined only once under a strict global budget. We present *Cascaded Transfer Learning* (CTL), a new approach that lies at the middle ground between MTL and TL (Table 1). Rather than adapting a source model directly to each target task, CTL propagates knowledge through a sequence of tasks (Figure 1). The key idea is that coordinated transfer across a graph structure connecting the tasks, and more specifically minimum spanning trees (MSTs), can realize gains compared to independent direct adaptations. To the best of our knowledge, this is the first work to provide such a framework for cascaded transfer over large task collections under budget constraints¹. Our contributions can be summarized as follows:

- (i) We provide a theoretical analysis of cascaded transfer over trees, establishing sufficient conditions under which CTL provably improves over direct transfer.
- (ii) Building on this analysis, we present a scalable CTL algorithm that constructs a transfer tree and allocates a

¹We should remark that the term ‘‘cascade’’ has been used in prior TL works in diverse ways, which however are conceptually different from the CTL framework.

Table 1. Positioning CTL relative to MTL and TL in the frugal many-task learning regime.

	MTL	TL	CTL
Training	Joint, iterative	Independent per task	Sequential cascade
Information flow	Shared parameters	Source to each target	Cascade over task graph
Task updates	Multiple (revisting)	Once (fine-tuning)	Once (single-pass)
Budget	Joint training cost	Per-task independent	Global shared allocation
Interaction type	Implicit via shared parameters	Direct source-to-target	Explicit, distance-based task graph
Error propagation	Coupled via shared parameters	Single-step bias	Path-dependent cascade
Scalability	Limited (interaction overhead)	High (parallel)	High (sequential, parallel per branch)

limited training budget across tasks.

2. Cascaded Transfer Learning

This section formalizes CTL, introduces the underlying task-dependency structure, and describes practical strategies for constructing cascades under budget constraints.

2.1. Preliminaries

Let \mathcal{V} be a set of tasks, with cardinality $|\mathcal{V}|$. For two tasks $u, v \in \mathcal{V}$, we write $u \rightarrow v$ to denote a transfer from task u to task v . Let $n \in \mathbb{N}^*$ be the number of samples available and $d \in \mathbb{N}^*$ the feature dimension, such that for each task $v \in \mathcal{V}$, $\mathbf{X}_v \in \mathbb{R}^{n \times d}$ denote the task-specific data matrix. Each task is associated with an unknown parameter vector $\theta_v^* \in \mathbb{R}^d$ to be learned from data. Let $b_v \in \mathbb{N}^*$ denote the computational budget allocated to that task, i.e. a fixed amount of local optimization effort, measured in refinement steps. Similar notions of computational budget have been used in prior work on learning under constrained optimization effort (Wong et al., 2021).

Let $G_v^b : \mathbb{R}^d \rightarrow \mathbb{R}^d$ be a refinement operator corresponding to b iterations of a gradient-based optimization algorithm applied to a parameter vector. Given a source task u and a target task v , a transfer $u \rightarrow v$ consists of initializing the parameters of v using information from u , followed by local refinement via G_v^b . This source–target adaptation forms the elementary building block of our framework, which extends such transfers to a graph-structured setting. In that regard, a central object is the *rooted tree* $\mathcal{T}_s = (\mathcal{V}, \mathcal{E}, s)$, where \mathcal{E} is the set of edges and s the *root*. A rooted tree is a *directed acyclic graph* (DAG) where each node has at most one parent, denoted by $\text{pa}(v)$. For convenience, we make the convention that $\text{pa}(s)$ is a dummy node corresponding to a model with random parameters θ_{init} .

2.2. The Cascaded Transfer Learning Paradigm

We now formalize CTL, starting from the rooted tree setting.

Definition 2.1. *Cascaded Transfer Learning* is a learning process in which tasks in a set \mathcal{V} are learned sequentially following the structure of a rooted tree $\mathcal{T}_s = (\mathcal{V}, \mathcal{E}, s)$ that connects them. Starting from the root s , each subsequent task is initialized by its parent and is then locally refined.

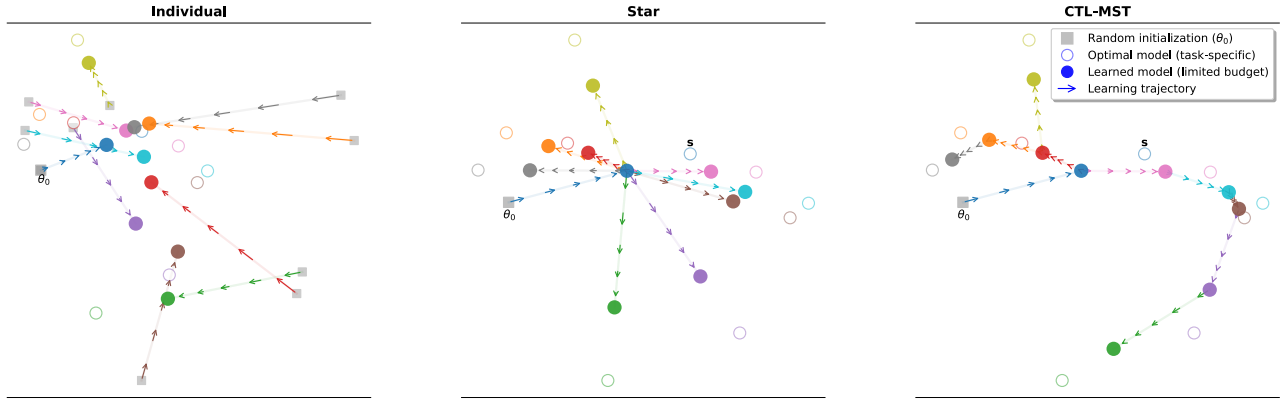


Figure 1. Parameter-space intuition for CTL. Arrows are shown along learning trajectories associated to different tasks (i.e. iterative parameter optimization). Each learning trajectory has a distinct color and stops at a learned model (solid nodes) that is short of its optimum (white-filled nodes) due to the limited available training budget. *Left:* Independent training. Each task is optimized from its own initialization. *Middle:* Star transfer. One source task is learned first and directly transferred to all other tasks. *Right:* CTL where tasks are learned sequentially along a minimum spanning tree. Long transfers are realized by a series steps involving intermediate tasks.

Algorithm 1 Cascaded Transfer Learning

```

1: Input: set of tasks  $\mathcal{V} = \{v_1, v_2, \dots\}$ , total training budget  $B$ , undirected task graph  $\mathcal{G}$ 
2: Output: refined models  $\{\tilde{\theta}_v\}_{v \in \mathcal{V}}$ 
3: Seed selection: choose the root task  $s \in \mathcal{V}$ 
4: Tree construction: construct a rooted tree  $\mathcal{T}_s = (\mathcal{V}, \mathcal{E}, s)$  from the graph  $\mathcal{G}$ 
5: Budget allocation: assign budgets  $\{b_v\}_{v \in \mathcal{V}}$ ,  $\sum_{v \in \mathcal{V}} b_v = B$ 
6: Cascaded transfer:
7:   initialize  $\theta_{\text{pa}(s)}$  with random  $\theta_{\text{init}}$ 
8:   for each task  $v \in \mathcal{T}_s$  in topological order do
9:     set  $\theta_v^{(0)} = \tilde{\theta}_{\text{pa}(v)}$ 
10:    Refine:  $\tilde{\theta}_v = G_v^{b_v}(\theta_v^{(0)})$ 
11:   endfor
12: Return:  $\{\tilde{\theta}_v\}_{v \in \mathcal{V}}$ 

```

Figure 1 illustrates the rationale of the CTL framework, and how, starting from a chosen seed, information is propagated from task to task along the cascade. Algorithm 1 gives the pseudocode that involves three central design choices:

- (i) *Seed selection.* The root task s that initiates the cascade.
- (ii) *Graph construction.* Building a rooted tree from a weighted task graph \mathcal{G} , whose edge weights encode pairwise task distances and determine the direction and locality of information flow.
- (iii) *Budget allocation and refinement.* The assignment of refinement budgets $\{b_v\}_{v \in \mathcal{V}}$ and the execution of local optimization along the cascade.

Cascade Construction Strategies. Rather than treating transfers independently, CTL organizes and performs them by following a predefined graph structure connecting the tasks. A central question is what should this structure be so that routing information through intermediate tasks is

globally beneficial.

At a local level, consider three tasks (S, I, T) , where S is already learned and I and T remain to be refined. A natural baseline is to transfer directly and independently from S to each task, $S \rightarrow I$ and $S \rightarrow T$. However, when a fixed limited budget is available and I is relevant to T , this strategy may be suboptimal in learning both I and T , compared to the path $S \rightarrow I \rightarrow T$. In that case, the refinement of I not only improves its own estimate, but also produces a good initialization for T , effectively decomposing a long transfer into a sequence of shorter, more reliable steps. This mechanism, illustrated by the chained learning trajectories in Figure 1, allows information to propagate progressively while respecting the budget constraint. Section 3 gives the conditions under which the error introduced by intermediate step remains controlled and accumulates favorably along a path. In particular, when local optimization procedures are stable and task distances are sufficiently small, cascaded transfer can outperform direct transfers executed independently. In those cases, it becomes natural to organize learning through a global structure that connects neighboring tasks while supporting propagation through intermediates. Rooted trees provide a simple and effective realization of this principle.

Tree construction is contingent upon the quality and semantics of the input task graph \mathcal{G} , which encodes prior information about task relationships and directly governs the direction and locality of information flow in the cascade. When an application-specific task graph is available (e.g., induced by spatial proximity, network topology, or known hierarchies) it can be provided directly as input. Otherwise, task relationships must be inferred from data, typically through noisy proxies such as empirical features, gradients,

or learned representations, yielding a weighted task graph constructed from pairwise task distances.

Default Tree Construction. To instantiate CTL in practice in a fully data-driven way, we need to have access to a task distance matrix, and then specify the cascade root and its tree structure. The task geometry encodes task transferability and enables the cascade tree construction. This information is not directly accessible in practice, one needs to consider ways to compute empirical task distances to approximate it. This is explored experimentally in Section 4. Starting from the complete graph induced by a given pairwise task distance matrix, we consider an MST, which is an undirected graph that connects all tasks while minimizing the total edge weight, corresponding to the sum of pairwise task distances. By the assumption that task distances are good proxies for transfer difficulty (i.e., potentially higher estimation error at the target task when initializing it by a neighboring task), we can deduce that an MST is a good proxy for handling the overall cascaded transfer problem. Setting a root to an MST affects the traversal, but not the quality of the tree (Kleinberg & Tardos, 2006), and consequently does not also affect the estimation error of MST-based CTL. We choose though the medoid as a seed, which is an actual task having minimal sum of pairwise distances to the other tasks. Rooting MSTs at the medoid task is outlier-resistant, also tends to produce more balanced and shallow trees, making the cascade less sequential and hence requiring less total computational time.

Computational Complexity. The computational cost of CTL is dominated by the construction of the cascade structure from the input task graph. In general, CTL operates on an undirected task graph \mathcal{G} , from which an MST is extracted. The cost of building the MST depends on the size and sparsity of \mathcal{G} : for a dense graph specified by pairwise relations, this step requires $\mathcal{O}(|\mathcal{V}|^2 \log |\mathcal{V}|)$ time, incurred only once prior to the cascade, while sparser graphs yield lower complexity. Once the cascade is constructed, training proceeds locally along the tree: each task is refined exactly once from its parent, and the total optimization cost scales linearly with the global refinement budget. As a result, the dominant cost during deployment is governed by budgeted local updates rather than by joint or repeated task optimization.

Extensions. The abstract CTL framework can be naturally generalized in a number of directions that we mention here, although their proper investigation is out of the scope of this paper. First, while our presentation is restricted to a single rooted tree, the same principles apply to a *cascade forest* in which multiple seeds initiate independent cascades over disjoint subsets of tasks. Deciding when more than one seed would be beneficial and selecting those seeds, is itself a design problem that can be informed by task distances, clustering criteria, or transferability estimates.

Second, Definition 2.1 can be stated more generally for DAGs, which include rooted trees. That would allow a task to fuse information from multiple parents.

3. Theoretical Analysis

We justify CTL over rooted trees for the many task learning objective. Our analysis shows that: (i) tree-structured cascades can improve over independent or pairwise transfer by routing long-range transfers through sequences of shorter ones in terms of task distance, (ii) only mild structural conditions on the tree are required, and (iii) rooted distance-based trees such as MSTs naturally satisfy these conditions when task distances are assumed given in hindsight.

Notations. The Euclidean and Frobenius norms are denoted by $\|\cdot\|$ and $\|\cdot\|_F$. The positive definiteness of a symmetric matrix \mathbf{S} is expressed as $\mathbf{S} \succ 0$. With $B \in \mathbb{N}^*$ we denote the total learning budget. Given a rooted tree \mathcal{T}_s and a budget allocation $\{b_v\}_{v \in \mathcal{V}}$ satisfying $\sum_{v \in \mathcal{V}} b_v = B$, CTL refines tasks following the topological (root-to-leaf) order, with updates of the form $\tilde{\boldsymbol{\theta}}_v = G_v^{b_v}(\tilde{\boldsymbol{\theta}}_{\text{pa}(v)})$.

3.1. Parameter-Space Analysis

For each task $v \in \mathcal{V}$, we associate a loss $\mathcal{L}_v : \mathbb{R}^d \rightarrow \mathbb{R}$ and a minimizer $\boldsymbol{\theta}_v^* \in \mathbb{R}^d$. Let $\eta \in (0, 1)$ be the learning step associated to the refinement operator G_v . We assume a contraction property in the parameter space: for all $v \in \mathcal{V}$, there exists a contraction rate $\rho_v \in (0, 1)$ such that, for all $(\boldsymbol{\theta}, b) \in \mathbb{R}^d \times \mathbb{N}^*$,

$$\|G_v^b(\boldsymbol{\theta}) - \boldsymbol{\theta}_v^*\| \leq \rho_v^b \|\boldsymbol{\theta} - \boldsymbol{\theta}_v^*\|.$$

This condition ensures that each local refinement step reduces estimation error at a geometric rate. It holds, for instance, for gradient descent on strongly convex and smooth objectives, and serves as a sufficient condition for controlling error accumulation along a cascade.

We further assume the existence of a latent task geometry that governs transfer difficulty. Specifically, we measure the discrepancy between two tasks u and v by $d(u, v) = \|\boldsymbol{\theta}_u^* - \boldsymbol{\theta}_v^*\|$, and interpret this distance as a proxy for the bias incurred when transferring from u to v . While this distance is not directly observable in practice, it provides a conceptual model for how task mismatch affects transfer. Under the contraction assumption above, initializing task v from a solution close to $\boldsymbol{\theta}_u^*$ induces an estimation error at v that is proportional to $d(u, v)$ up to a contraction factor.

Proposition 3.1 (Cascaded transfer over a path). *For any task $v \neq v_0$, and a path $(v_0 \rightarrow v_1 \rightarrow \dots \rightarrow v_m = v)$, involving $m > 1$ intermediate nodes, it holds:*

$$\|\tilde{\boldsymbol{\theta}}_v - \boldsymbol{\theta}_v^*\| \leq P_{1:m} \|\tilde{\boldsymbol{\theta}}_{v_0} - \boldsymbol{\theta}_{v_0}^*\| + \sum_{i=1}^m P_{i:m} d(v_{i-1}, v_i),$$

where $P_{i:m} = \prod_{j=i}^m \rho_{v_j}^{b_{v_j}}$ is a multiplicative attenuation factor.

As a result, the contribution of each edge of a path is progressively attenuated by downstream refinement. The above bound shows that CTL improves over direct transfer when: (i) graph edges connect nearby tasks (locality), (ii) the structure is acyclic and ordered, (iii) budgets prevent error accumulation along deep paths. Importantly, these conditions depend on inter-task distances but do not uniquely determine an optimal transfer structure, since the effective contribution of an edge also depends on its position in the cascade through downstream discounting, which is unknown prior to constructing the tree. When only pairwise distances are available, minimizing cumulative edge lengths provides a principled and tractable approximation. In this setting, minimum spanning trees enforce locality, are acyclic by construction, and are stable to noise in similarity estimates, making them a robust default for constructing CTL cascades.

CTL vs TL. Why Cascades? The central question is whether routing transfer through intermediate tasks can reduce the error induced by task mismatch, under a fixed refinement budget. The following result formalizes this intuition by isolating the *transfer bias* induced by task geometry.

Theorem 3.2. *Suppose a path $(s \rightarrow v_1 \rightarrow \dots \rightarrow v_m = v)$ starting from an exact task, $\theta_s = \theta_s^*$, and having uniform refinement budget b at each other node. Let $\delta_i = d(v_{i-1}, v_i)$, $\delta_{\max} = \max_{1 \leq i \leq m} \delta_i$, and $\rho_{\max} = \max_{1 \leq i \leq m} \rho_{v_i}$.*

The estimation errors of the cascaded transfer along the path and that of direct transfer $s \rightarrow v$ are:

$$\begin{aligned} \|\tilde{\theta}_v^{\text{CTL}} - \theta_v^*\| &\leq \sum_{i=1}^m \rho_{v_i}^{(m-i+1)b} \delta_i, \\ \|\tilde{\theta}_v^{\text{TL}} - \theta_v^*\| &\leq \rho_v^b d(s, v). \end{aligned}$$

CTL has a tighter upper bound than TL when:

$$\delta_{\max}(1 - \rho_{\max}^{mb}) < d(s, v)(1 - \rho_{\max}^b).$$

Theorem 3.2 highlights a fundamental distinction between cascaded and direct transfer. Star transfer incurs a single estimation error proportional to the pairwise distance $d(s, v)$ between the source and the target, which is discounted only once by the local refinement. In contrast, CTL decomposes this mismatch into a sequence of local discrepancies $\delta_i = d(v_{i-1}, v_i)$, each of which is further attenuated by all downstream refinements. As a result, when tasks vary smoothly along the cascade (small δ_i), the discounted sum of local errors is strictly smaller than the discounted direct source-target transfer. This explains why locality-preserving trees are effective: CTL exploits gradual variations in task geometry rather than relying on a single direct transfer between distant tasks.

3.2. Feature-Space Analysis

We now consider the linear feature-space setting with random design and $n \geq d$. For each task $v \in \mathcal{V}$, let $\mathbf{X}_v \in \mathbb{R}^{n \times d}$, and $\mathbf{y}_v \in \mathbb{R}^n$. We consider the quadratic objective $\mathcal{L}_v(\theta) = \frac{1}{2} \|\mathbf{X}_v \theta - \mathbf{y}_v\|^2$, $\theta \in \mathbb{R}^d$. A single gradient descent step with step size $\eta > 0$ yields the affine update $G_v(\theta) = \mathbf{M}_v \theta + \eta \mathbf{X}_v^\top \mathbf{y}_v$, where $\mathbf{M}_v = \mathbf{I}_d - \eta \mathbf{X}_v^\top \mathbf{X}_v$.

We assume that $\mathbf{X}_v^\top \mathbf{X}_v \succ 0$, and choose a step size $\eta \in (0, 2/\lambda_{\max}(\mathbf{X}_v^\top \mathbf{X}_v))$, where λ_{\max} is its largest eigenvalue. Under this condition, the linear operator $\mathbf{M}_v = \mathbf{I}_d - \eta \mathbf{X}_v^\top \mathbf{X}_v$ satisfies $\|\mathbf{M}_v\| = \rho_v < 1$, and therefore the refinement operator G_v is a contraction on $(\mathbb{R}^d, \|\cdot\|)$. We further assume a linear model: for each task $v \in \mathcal{V}$, we model \mathbf{y}_v as:

$$\mathbf{y}_v = \mathbf{X}_v \theta_v^*,$$

where $\theta_v^* \in \mathbb{R}^d$. In this setting, gradient-based refinement contracts toward the task-specific optimum θ_v^* , and the same edge-wise and path-wise propagation bounds as in parameter space apply directly.

Under the above feature-space contraction assumptions, the same edge-wise and path-wise error propagation guarantees hold as in the parameter space continue. Cascaded transfer therefore progressively aligns feature representations across tasks, with downstream contractions correcting both inherited error and feature mismatch. This provides an intuitive explanation for the stability of cascades built from feature-based distances and motivates their use in practice.

Noisy Feature-Space Analysis. We now extend the noiseless linear model to include additive observation noise. For each task $v \in \mathcal{V}$, we now model \mathbf{y}_v as a random variable taking values in \mathbb{R}^n such that:

$$\mathbf{y}_v = \mathbf{X}_v \theta_v^* + \varepsilon_v,$$

where ε_v has independent, mean-zero, sub-Gaussian coordinates, and $\theta_v^* \in \mathbb{R}^d$ is the task-specific optimum.

We assume that the feature-space contraction condition holds for a suitable step size $\eta > 0$. As previously, gradient-based refinement induces a contraction toward a task-dependent optimum. In the presence of observation noise, however, this contraction occurs toward the empirical minimizer $\hat{\theta}_v = \arg \min_{\theta \in \mathbb{R}^d} \frac{1}{2} \|\mathbf{X}_v \theta - \mathbf{y}_v\|^2$, rather than toward the population parameter θ_v^* . The discrepancy $\|\hat{\theta}_v - \theta_v^*\|$ captures the statistical estimation error and perturbs the task geometry induced by the feature space. In expectation, the magnitude of this perturbation is controlled by the conditioning of the task-specific design through the linear operator $\mathbf{A}_v = (\mathbf{X}_v^\top \mathbf{X}_v)^{-1} \mathbf{X}_v^\top$, which governs how noise propagates from data space to parameter space.

Proposition 3.3 (Expected noisy propagation along a path). *Under the noisy linear model and the feature-space contraction assumption, the expected estimation error propagated along a path admits the following bound. Using the same notation as in Proposition 3.1, it holds:*

$$\begin{aligned} \mathbb{E} [\|\tilde{\theta}_v - \theta_v^*\|] &\leq P_{1:m} \mathbb{E} [\|\tilde{\theta}_s - \theta_s^*\|] \\ &+ \sum_{i=1}^m P_{i:m} d(v_{i-1}, v_i) \\ &+ \sum_{i=1}^m P_{i+1:m} \sigma_{v_i} \left(1 + \rho_{v_i}^{b_{v_i}}\right) \|\mathbf{A}_{v_i}\|_F. \end{aligned}$$

All expectations are taken with respect to the observation noise $\{\varepsilon_v\}_{v \in \mathcal{V}}$. This bound shows that, in expectation, CTL decomposes the final error into two discounted components: a bias term, and a noise term capturing the propagation of estimation error. As in the noiseless setting, locality reduces transfer bias, while sufficient downstream refinement or shallow cascades limit noise accumulation.

4. Experiments

The goal of our experiments is to demonstrate that CTL effectively exploits task-graph structure to improve performance under a fixed or reduced computational budget, and to show that these gains are not specific to a particular data modality or learning problem. We therefore evaluate CTL across diverse settings, including synthetic and real-world regression, as well as image-based classification tasks. Across all experiments, learning follows the same paradigm. Each task is associated with a local objective and is optimized independently using gradient-based methods. Task interactions occur exclusively through parameter initialization: each node in the cascade is initialized by its parent in the tree, and then local refinement takes place.

4.1. Datasets

Synthetic and real-world datasets are used to evaluate CTL under controlled heterogeneity and realistic conditions.

Synthetic Dataset. We construct families of linear regression tasks of the form $\mathbf{y}_v = \mathbf{X}_v \theta_v + \varepsilon_v$, where $\mathbf{X}_v \in \mathbb{R}^{n \times d}$ has i.i.d. standard Gaussian rows and $\varepsilon_v \sim \mathcal{N}(\mathbf{0}, \sigma^2 \mathbf{I}_n)$, with $\sigma > 0$. To control task relatedness, we consider the following generative model: we first draw a global center θ_0 and K cluster shifts $\delta_c \sim \mathcal{N}(\mathbf{0}, \tau_{\text{between}}^2 \mathbf{I}_d)$, every task v is assigned a cluster $c(v)$ and its parameter is generated as $\theta_v = \theta_0 + \delta_{c(v)} + \zeta_v$ with $\zeta_v \sim \mathcal{N}(\mathbf{0}, \tau_{\text{within}}^2 \mathbf{I}_d)$. Varying τ or $(\tau_{\text{within}}, \tau_{\text{between}})$ controls the degree and structure of heterogeneity, enabling systematic evaluation across regimes ranging from nearly homogeneous tasks to well-separated clusters, see Figure 5 in Appendix.

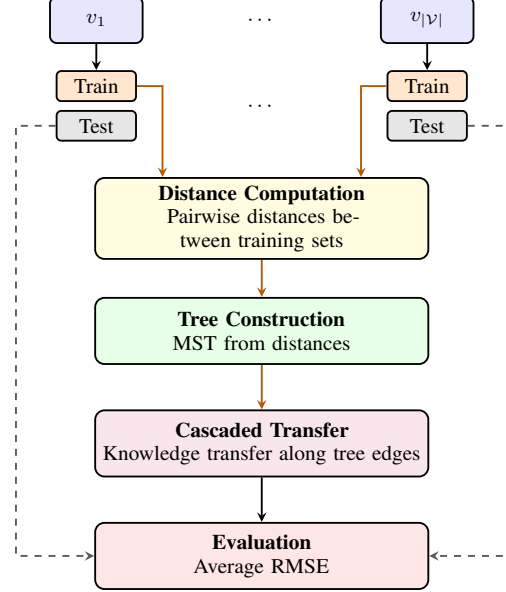


Figure 2. Experimental protocol. The dataset of each task v_i is split into train/test sets. Training-phase components (distance computation, tree construction, cascaded transfer) operate solely on training data. Final evaluation uses held-out test sets, with results averaged over 50 random seeds.

Real Datasets. We evaluate CTL on both time-series forecasting and image classification. For time-series regression, we use the UK electricity dataset², which provides aggregated half-hourly residential demand from smart meters operated by two major UK distribution network operators. We focus on a subset of 100 nodes in the Oxford urban area and predict feeder-level demand using calendar features and lagged load values. To assess generality beyond regression, we also consider high-dimensional image classification tasks derived from Fashion-MNIST and CIFAR-10. Each task corresponds to a binary classification problem defined over a pair of classes, and multiple related tasks are obtained by training on different subsets of the data. This setting yields collections of closely related but non-identical tasks, making it well suited for evaluating cascaded transfer learning in classification regimes.

4.2. Experimental Settings

For all regression experiments, datasets are split into disjoint training and test sets. In the synthetic setting, we use fixed sizes of $n_{\text{train}} = 64$ and $n_{\text{test}} = 128$ per task. For the real-world time-series dataset, the training set spans from February 14, 2024, at 12:00 a.m. to February 24, 2024, at 11:30 p.m., while the test set spans from February 25, 2024, at 12:00 a.m. to February 28, 2024, at 11:30 p.m. For image classification experiments, each task is trained and evaluated

²<https://weave.energy/>

using fixed-size train and test splits, and all methods use the same model architecture and optimization hyperparameters across tasks. In all cases, task graphs are constructed from training data. Models are evaluated on the test set using the same metrics (root mean squared error) across all methods, and all results are averaged over 50 random seeds to account for variability due to data sampling and initialization. This experimental protocol is summarized in Figure 2.

4.3. Baselines

We compare our approach with several tree-structured or non-transfer baselines. All methods use identical training routines, both for seed training and local refinement.

- *Individual models*. For each task, an individual model is trained independently for a fixed computational budget. This serves as a baseline without multi-task or transfer learning.
- *Star Tree*. A seed task s is selected, and then a star graph is constructed: $(s \rightarrow v)$, for all v . Each node receives the seed parameters and performs independent refinement.
- *Random Tree*. A seed task s is selected, and a random spanning tree over all tasks is generated by sampling a Prüfer sequence uniformly (Kumar et al., 1998; Deo & Micikevicius, 2001), which yields a labeled tree drawn uniformly from the set of all spanning trees. The tree is then rooted at s by orienting all edges away from it. This baseline represents an uninformed hierarchical transfer structure that does not exploit any task-related information.
- *Minimum Spanning Tree*. We consider several MST-based cascades that differ only in the task distance used to construct the tree. We evaluate distances based on target similarity, feature representations, optimization geometry (gradient or model-based), and distributional or representation-level discrepancies (Lv et al., 2024). Full definitions of the distance metrics are provided in the appendix.

4.4. Results

Table 3 and Figure 3 provide a unified view of all experiments across synthetic regression, UK electricity forecasting, and image classification, enabling direct comparison of transfer structures, task geometries, and budgets.

Synthetic regression. Across all regimes, cascaded transfer consistently outperforms independent training and shallow baselines, confirming that exploiting task structure remains beneficial even under increasing heterogeneity. At low to moderate variability, distances aligned with the underlying optimization or model geometry (for instance, gradient and parameter-based) yield the lowest errors across budgets, leading to improvements of 20–35% relative to independent training. As heterogeneity increases ($\tau = 10$), absolute gains diminish and variance grows, reflecting weaker task relatedness; nevertheless, optimization-aligned distances

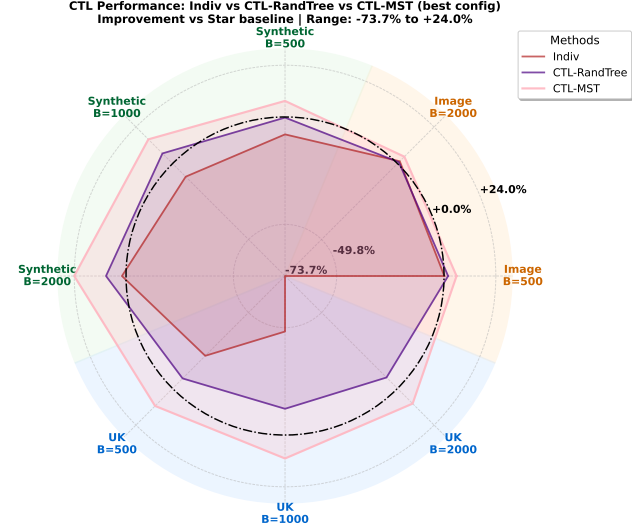


Figure 3. Radar plot of average improvement (%) as compared to the Star baseline, across datasets and budgets.

remain systematically superior to purely feature-based or uninformed measures. Distributional distances provide competitive but less stable performance, while feature-based distances degrade more rapidly with increasing dispersion.

UK electricity forecasting. Across all settings, independent training yields the highest errors, highlighting the limitations of learning tasks in isolation. Shallow star-shaped transfer improves performance but exhibits higher variance and degrades in low-budget regimes, indicating sensitivity to unfavorable source–target mismatches. In contrast, cascaded transfer consistently reduces RMSE across budgets, with distances aligned to target or optimization geometry delivering the most stable gains. At low budget, cascaded transfer reduces RMSE by more than 25% relative to independent training, while at higher budget reductions approach 50%. The aggregate results in Figure 3 confirm that geometry-aware distances consistently outperform unstructured or feature-only measures, demonstrating that cascaded transfer effectively amortizes optimization effort across related forecasting tasks under tight computational constraints.

Image classification. On Fashion-MNIST, cascaded transfer consistently improves over independent training and shallow baselines across the budget range. Distances based on gradients or task-level feature statistics yield the most stable improvements, particularly in low-budget regimes where cascaded initialization compensates for limited task-specific optimization. In contrast, random hierarchies and star-shaped transfer provide only marginal gains, underscoring the importance of task geometry. On CIFAR-10, improvements are smaller and variability is higher, reflecting increased task difficulty and weaker inter-task alignment. Nevertheless, cascaded transfer remains beneficial

Table 2. Results with MST-based cascaded transfer aggregated by distance family (Feature, Target, Optimization) across different number of tasks T and global budget B . Values are averaged over distance variants within each family. Lower is better for RMSE and higher is better for accuracy. **Bold** and underlined entries denote best and second-best performance *within each row*.

Dataset	Params		Indiv	Baselines		Feature	CTL-MST	
	T	B		Star	CTL-RandTree		Target	Optimization
Synthetic Regression (RMSE)								
Syn-10	200	500	913.8 ± 168.4	845.5 ± 178.8	872.5 ± 253.1	840 ± 215	853 ± 228	825 ± 221
Syn-10	200	1000	871.5 ± 141.6	802.4 ± 189.5	749.2 ± 171.0	752 ± 188	758 ± 176	694 ± 161
Syn-10	200	2000	912.8 ± 174.3	930.2 ± 262.4	887.2 ± 246.1	846 ± 228	<u>809 ± 221</u>	715 ± 178
UK Electricity Forecasting (RMSE, kWh)								
UK	100	500	2729.4 ± 8.8	2247.9 ± 51.8	2395.9 ± 59.4	2391 ± 51	2086 ± 49	2040 ± 42
UK	100	1000	2694.4 ± 9.5	1820.7 ± 38.7	2042.4 ± 36.4	1993 ± 38	<u>1695 ± 26</u>	1675 ± 26
UK	100	2000	2612.8 ± 7.3	1504.1 ± 19.0	1612.4 ± 16.3	1612 ± 19	<u>1388 ± 8</u>	1375 ± 7
Image Classification (Accuracy, %)								
FMNIST	200	500	90.6 ± 5.2	90.5 ± 5.2	91.5 ± 4.1	93.6 ± 3.6	90.4 ± 4.9	<u>92.8 ± 4.2</u>
FMNIST	200	2000	94.5 ± 3.0	94.4 ± 3.3	94.1 ± 3.2	95.1 ± 3.1	94.0 ± 3.7	<u>95.1 ± 3.0</u>
CIFAR	200	500	60.9 ± 4.7	64.0 ± 4.3	65.2 ± 3.9	66.0 ± 3.8	64.8 ± 3.8	66.6 ± 3.7
CIFAR	200	2000	67.7 ± 3.9	66.7 ± 3.8	67.3 ± 3.5	67.9 ± 3.6	67.1 ± 3.9	68.6 ± 3.7

across most settings. While no single distance dominates uniformly, the results confirm that exploiting task geometry through cascaded transfer yields systematic accuracy gains even in challenging, high-dimensional classification.

Summary. Across regression, forecasting, and classification tasks, the results confirm that organizing transfer through a tree yields robust and consistent improvements over both no-transfer and shallow-transfer baselines. Within cascaded transfer, the choice of task distance is critical: distances aligned with the underlying optimization or target geometry consistently outperform purely feature-based or uninformed measures across datasets and budgets. These findings closely match the theoretical analysis, which predicts that routing transfer through local, geometry-aware cascades mitigates the bias incurred by long-range transfer under constrained budgets.

5. Conclusion and Perspectives

We introduced *Cascaded Transfer Learning*, a framework for many-task learning under a strict global budget. CTL formulates knowledge transfer as a structured propagation process over a rooted tree, in which tasks are refined sequentially rather than jointly optimized. This design enables controlled information flow across tasks and departs from both independent training and shallow transfer schemes.

We provided a theoretical analysis of error propagation along cascades, establishing sufficient conditions under which routing transfer through intermediate tasks improves over direct transfer. The analysis clarifies how task distances, local optimization stability, and cascade depth jointly govern transfer bias and variance, and applies broadly across parameter and feature-space settings, including noisy regimes.

Empirically, CTL consistently outperforms independent and star-shaped baselines on synthetic regression, electricity forecasting, and image classification. Simple geometry-based constructions such as minimum spanning trees emerge as robust and effective defaults, yielding reliable gains under realistic heterogeneity. Overall, CTL offers a principled and computationally efficient approach to structured knowledge transfer, and provides a foundation for further research on resource-aware many-task learning.

Future directions include extending CTL to nonlinear models and deep representations, as well as to more general cascade structures beyond trees. Another promising avenue is the development of adaptive budget allocation strategies that account for task difficulty or uncertainty.

Impact Statement

This work advances Machine Learning by studying scalable transfer mechanisms across large collections of related tasks. The proposed Cascaded Transfer Learning framework emphasizes computational frugality: tasks are refined locally under an explicit global budget, avoiding repeated joint optimization or large-scale retraining. By favoring lightweight, localized updates over centralized training, CTL reduces redundant computation and can lower energy consumption in many-task and distributed learning settings.

References

Antoniadis, A., Gaucher, S., and Goude, Y. Hierarchical transfer learning with applications to electricity load forecasting. *International Journal of Forecasting*, 40:641–660, 2024.

Aribandi, V., Tay, Y., Schuster, T., Rao, J., Zheng, H. S., Mehta, S. V., Zhuang, H., Tran, V. Q., Bahri, D., Ni, J., et al. ExT5: Towards extreme multi-task scaling for transfer learning. In *International Conference on Learning Representations*, 2022.

Ciliberto, C., Mroueh, Y., Poggio, T., and Rosasco, L. Convex learning of multiple tasks and their structure. In *International Conference on Machine Learning*, pp. 1548–1557, 2015.

Deo, N. and Micikevicius, P. Prufer-like codes for labeled trees. *Congressus Numerantium*, pp. 65–74, 2001.

Fallah, A., Mokhtari, A., and Ozdaglar, A. Personalized federated learning with theoretical guarantees: a model-agnostic meta-learning approach. In *Advances in Neural Information Processing Systems*, 2020.

Hashimoto, K., Xiong, C., Tsuruoka, Y., and Socher, R. A joint many-task model: Growing a neural network for multiple NLP tasks. In *Conference on Empirical Methods in Natural Language Processing*, pp. 1923–1933, 2017.

He, X., Alesiani, F., and Shaker, A. Efficient and scalable multi-task regression on massive number of tasks. In *AAAI Conference on Artificial Intelligence*, volume 33, pp. 3763–3770, 2019.

Kleinberg, J. and Tardos, E. *Algorithm Design*. Addison-Wesley, 2006.

Kolesnikov, A., Beyer, L., Zhai, X., Puigcerver, J., Yung, J., Gelly, S., and Houlsby, N. Big transfer (bit): General visual representation learning. In *European Conference on Computer Vision*, pp. 491–507, 2020.

Kornblith, S., Shlens, J., and Le, Q. V. Do better imagenet models transfer better? In *IEEE/CVF Conference on Computer Vision and Pattern Recognition*, pp. 2661–2671, 2019.

Kumar, V., Deo, N., and Kumar, N. Parallel generation of random trees and connected graphs. *Congressus Numerantium*, pp. 7–18, 1998.

Laptev, N., Yu, J., and Rajagopal, R. Applied timeseries transfer learning. In *International Conference on Learning Representations – Workshop Track*, 2018.

Li, T., Hu, S., Beirami, A., and Smith, V. Ditto: Fair and robust federated learning through personalization. In *International Conference on Machine Learning*, pp. 6357–6368, 2021.

Liu, J., Xia, Z., Lei, Y., Li, X., and Wang, X. Multi-faceted hierarchical multi-task learning for a large number of tasks with multi-dimensional relations. *Preprint arXiv:2110.13365*, 2021.

Lv, J., Yang, H., and Li, P. Wasserstein distance rivals Kullback-Leibler divergence for knowledge distillation. In *Advances in Neural Information Processing Systems*, volume 37, pp. 65445–65475, 2024.

Mouatadid, S., Orenstein, P., Flaspohler, G., Oprescu, M., Cohen, J., Wang, F., Knight, S., Geogdzhayeva, M., Levang, S., Fraenkel, E., et al. SubseasonalclimateUSA: A dataset for subseasonal forecasting and benchmarking. *Advances in Neural Information Processing Systems*, 36: 7960–7992, 2023.

Pan, S. J. and Yang, Q. A survey on transfer learning. *IEEE Transactions on Knowledge and Data Engineering*, 22 (10):1345–1359, 2009.

Raffel, C., Shazeer, N., Roberts, A., Lee, K., Narang, S., Matena, M., Zhou, Y., Li, W., and Liu, P. J. Exploring the limits of transfer learning with a unified text-to-text transformer. *Journal of Machine Learning Research*, 21 (140):1–67, 2020.

Rasp, S., Hoyer, S., Merose, A., Langmore, I., Battaglia, P., Russell, T., Sanchez-Gonzalez, A., Yang, V., Carver, R., Agrawal, S., et al. WeatherBench 2: A benchmark for the next generation of data-driven global weather models. *Journal of Advances in Modeling Earth Systems*, 16(6), 2024.

Reddi, S., Charles, Z., Zaheer, M., Garrett, Z., Rush, K., Konečný, J., Kumar, S., and McMahan, H. B. Adaptive federated optimization. In *International Conference on Learning Representations*, 2021.

Ruiz, C., Alaíz, C. M., and Dorronsoro, J. R. A survey on kernel-based multi-task learning. *Neurocomputing*, 577: 127–255, 2024.

Sprangers, O., Wadman, W., Schelter, S., and de Rijke, M. Hierarchical forecasting at scale. *International Journal of Forecasting*, 40(4):1689–1700, 2024.

Standley, T., Zamir, A., Chen, D., Guibas, L., Malik, J., and Savarese, S. Which tasks should be learned together in multi-task learning? In *International Conference on Machine Learning*, pp. 9120–9132, 2020.

Strezoski, G., Noord, N. v., and Worring, M. Many task learning with task routing. In *IEEE/CVF International Conference on Computer Vision*, pp. 1375–1384, 2019.

Tan, Y., Zhang, E., Li, Y., Huang, S.-L., and Zhang, X.-P. Transferability-guided cross-domain cross-task transfer learning. *IEEE Transactions on Neural Networks and Learning Systems*, 2024.

Weiss, K., Khoshgoftaar, T. M., and Wang, D. A survey of transfer learning. *Journal of Big data*, 3(1):9, 2016.

Wong, C., Ellis, K. M., Tenenbaum, J., and Andreas, J. Leveraging language to learn program abstractions and search heuristics. In *International Conference on Machine Learning*, pp. 11193–11204, 2021.

Yu, J., Dai, Y., Liu, X., Huang, J., Shen, Y., Zhang, K., Zhou, R., Adhikarla, E., Ye, W., Liu, Y., et al. Unleashing the power of multi-task learning: A comprehensive survey spanning traditional, deep, and pretrained foundation model eras. *Preprint arXiv:2404.18961*, 2024.

Zhang, Y. and Yang, Q. An overview of multi-task learning. *National Science Review*, 5(1):30–43, 2018.

Zhang, Y. and Yang, Q. A survey on multi-task learning. *IEEE Transactions on Knowledge and Data Engineering*, 34(12):5586–5609, 2021.

Zhuang, F., Qi, Z., Duan, K., Xi, D., Zhu, Y., Zhu, H., Xiong, H., and He, Q. A comprehensive survey on transfer learning. *Proceedings of the IEEE*, 109(1):43–76, 2020.

A. Code Availability

To promote transparency and reproducibility, we provide an implementation of Cascaded Transfer Learning together with scripts to reproduce the experiments reported in this paper. The code and documentation are available through the project website at [this address](#).

B. Proofs for Theoretical Analysis of Cascaded Transfer Learning

B.1. Parameter-Space

Cascaded transfer over a path. By definition of the CTL update, $\tilde{\boldsymbol{\theta}}_v = G_v^{b_v}(\tilde{\boldsymbol{\theta}}_{\text{pa}(v)})$. By the contractive refinement assumption,

$$\|\tilde{\boldsymbol{\theta}}_v - \boldsymbol{\theta}_v^*\| = \|G_v^{b_v}(\tilde{\boldsymbol{\theta}}_{\text{pa}(v)}) - \boldsymbol{\theta}_v^*\| \leq \rho_v^{b_v} \|\tilde{\boldsymbol{\theta}}_{\text{pa}(v)} - \boldsymbol{\theta}_v^*\|.$$

Applying the triangle inequality,

$$\|\tilde{\boldsymbol{\theta}}_{\text{pa}(v)} - \boldsymbol{\theta}_v^*\| \leq \|\tilde{\boldsymbol{\theta}}_{\text{pa}(v)} - \boldsymbol{\theta}_{\text{pa}(v)}^*\| + d(\text{pa}(v), v).$$

Combining the two inequalities yields the result. \square

Path-wise error decomposition. Applying the above to node v_1 :

$$\|\tilde{\boldsymbol{\theta}}_{v_1} - \boldsymbol{\theta}_{v_1}^*\| \leq \rho_{v_1}^{b_{v_1}} \left(\|\tilde{\boldsymbol{\theta}}_{v_0} - \boldsymbol{\theta}_{v_0}^*\| + d(v_0, v_1) \right).$$

Same with node v_2 and substitute the previous inequality:

$$\|\tilde{\boldsymbol{\theta}}_{v_2} - \boldsymbol{\theta}_{v_2}^*\| \leq \rho_{v_1}^{b_{v_1}} \rho_{v_2}^{b_{v_2}} \|\tilde{\boldsymbol{\theta}}_{v_0} - \boldsymbol{\theta}_{v_0}^*\| + \rho_{v_1}^{b_{v_1}} \rho_{v_2}^{b_{v_2}} d(v_0, v_1) + \rho_{v_2}^{b_{v_2}} d(v_1, v_2).$$

Proceeding inductively, each application introduces a multiplicative factor $\rho_{v_i}^{b_{v_i}}$ on all upstream terms and adds a new edge term. Therefore, we introduce a multiplicative notation, for $i, m \in \mathbb{N}^*$, $P_{i:m} = \prod_{j=i}^m \rho_{v_j}^{b_{v_j}}$. Hence, we get

$$\|\tilde{\boldsymbol{\theta}}_v - \boldsymbol{\theta}_v^*\| \leq P_{1:m} \|\tilde{\boldsymbol{\theta}}_{v_0} - \boldsymbol{\theta}_{v_0}^*\| + \sum_{i=1}^m P_{i:m} d(v_{i-1}, v_i).$$

Setting $\tilde{\boldsymbol{\theta}}_{v_0} = \boldsymbol{\theta}_{v_0}^*$ cancels out the bias term, enforcing $b_{v_i} = b$ for all $1 \leq i \leq m$, plus bounding all ρ_{v_i} by ρ_{\max} and δ_i by δ_{\max} yields a finite geometric series of finite ratio ρ_{\max}^b . \square

B.2. Feature-Space

Feature-space contraction. The gradient update is $G_v(\boldsymbol{\theta}) = \boldsymbol{\theta} - \eta \mathbf{X}_v^\top (\mathbf{X}_v \boldsymbol{\theta} - \mathbf{y}_v) = \mathbf{M}_v \boldsymbol{\theta} + \eta \mathbf{X}_v^\top \mathbf{y}_v$. Since $\mathbf{y}_v = \mathbf{X}_v \boldsymbol{\theta}_v^*$ and $\boldsymbol{\theta}_v^*$ satisfies $\mathbf{X}_v^\top \mathbf{X}_v \boldsymbol{\theta}_v^* = \mathbf{X}_v^\top \mathbf{y}_v$, then $G_v(\boldsymbol{\theta}_v^*) = \boldsymbol{\theta}_v^*$, so $\boldsymbol{\theta}_v^*$ is a fixed point. Thus, $G_v(\boldsymbol{\theta}) - \boldsymbol{\theta}_v^* = \mathbf{M}_v(\boldsymbol{\theta} - \boldsymbol{\theta}_v^*)$. Iterating yields the claim. \square

Edge-wise propagation in feature space. The above yields $\tilde{\boldsymbol{\theta}}_v - \boldsymbol{\theta}_v^* = \mathbf{M}_v^{b_v}(\tilde{\boldsymbol{\theta}}_{\text{pa}(v)} - \boldsymbol{\theta}_v^*)$. Taking norms and using $\|\mathbf{M}_v^{b_v}\| \leq \rho_v^{b_v}$,

$$\|\tilde{\boldsymbol{\theta}}_v - \boldsymbol{\theta}_v^*\| \leq \rho_v^{b_v} \|\tilde{\boldsymbol{\theta}}_{\text{pa}(v)} - \boldsymbol{\theta}_v^*\|.$$

The result follows by the triangle inequality exactly as in the parameter-space case. \square

Path-wise error propagation in feature space. The argument follows verbatim from the parameter-space analysis. Unrolling the edge-wise inequality along the unique root-to- v path yields the stated bound, with each edge contribution geometrically damped by downstream refinements. \square

B.3. Noisy Feature-Space

Empirical optimum. The minimizer $\hat{\theta}_v$ of $\frac{1}{2}\|\mathbf{X}_v\theta - \mathbf{y}_v\|^2$ satisfies the equations

$$\mathbf{X}_v^\top \mathbf{X}_v \hat{\theta}_v = \mathbf{X}_v^\top \mathbf{y}_v = \mathbf{X}_v^\top (\mathbf{X}_v \theta_v^* + \varepsilon_v) = \mathbf{X}_v^\top \mathbf{X}_v \theta_v^* + \mathbf{X}_v^\top \varepsilon_v.$$

Since $\mathbf{X}_v^\top \mathbf{X}_v \succ 0$,

$$\hat{\theta}_v = \theta_v^* + (\mathbf{X}_v^\top \mathbf{X}_v)^{-1} \mathbf{X}_v^\top \varepsilon_v.$$

Equivalently, under Gaussian noise, the estimator $\hat{\theta}_v$ is normally distributed with mean θ_v^* and covariance $\sigma_v^2 \mathbf{A}_v \mathbf{A}_v^\top$. Moreover, the gradient update is $G_v(\theta) = \mathbf{M}_v \theta + \eta \mathbf{X}_v^\top \mathbf{y}_v$, with $\mathbf{M}_v = \mathbf{I}_d - \eta \mathbf{X}_v^\top \mathbf{X}_v$. Using $\mathbf{X}_v^\top \mathbf{y}_v = \mathbf{X}_v^\top \mathbf{X}_v \hat{\theta}_v$, we have that $\hat{\theta}_v$ is a fixed point. Hence $G_v(\theta) - \hat{\theta}_v = \mathbf{M}_v(\theta - \hat{\theta}_v)$, and iterating gives $G_v^{b_v}(\theta) - \hat{\theta}_v = \mathbf{M}_v^{b_v}(\theta - \hat{\theta}_v)$. \square

Expected estimation error. Let $\mathbf{A}_v = (\mathbf{X}_v^\top \mathbf{X}_v)^{-1} \mathbf{X}_v^\top$. From the empirical optimum lemma, $\hat{\theta}_v - \theta_v^* = \mathbf{A}_v \varepsilon_v$. Using Jensen's inequality yields $\mathbb{E}[\|\mathbf{A}_v \varepsilon_v\|] \leq \sqrt{\mathbb{E}[\|\mathbf{A}_v \varepsilon_v\|^2]}$. Now,

$$\|\mathbf{A}_v \varepsilon_v\|^2 = \varepsilon_v^\top \mathbf{A}_v^\top \mathbf{A}_v \varepsilon_v = \sum_{i,j} (\mathbf{A}_v^\top \mathbf{A}_v)_{ij} \varepsilon_{v,i} \varepsilon_{v,j}.$$

Since the coordinates are independent and mean-zero, $\mathbb{E}[\varepsilon_{v,i} \varepsilon_{v,j}] = 0$ for $i \neq j$. Therefore,

$$\mathbb{E}[\|\mathbf{A}_v \varepsilon_v\|^2] = \sum_i (\mathbf{A}_v^\top \mathbf{A}_v)_{ii} \mathbb{E}[\varepsilon_{v,i}^2] \leq \sigma_v^2 \sum_i (\mathbf{A}_v^\top \mathbf{A}_v)_{ii} = \sigma_v^2 \text{tr}(\mathbf{A}_v^\top \mathbf{A}_v) = \sigma_v^2 \|\mathbf{A}_v\|_F^2.$$

Combining yields $\mathbb{E}[\|\hat{\theta}_v - \theta_v^*\|] \leq \sigma_v \|\mathbf{A}_v\|_F$. \square

Expected noisy edge-wise propagation. With the contraction assumption for task v , we get

$$\|\tilde{\theta}_v - \hat{\theta}_v\| \leq \rho_v^{b_v} \|\tilde{\theta}_u - \hat{\theta}_v\|.$$

Then, using the triangle inequality,

$$\|\tilde{\theta}_u - \hat{\theta}_v\| \leq \|\tilde{\theta}_u - \theta_v^*\| + \|\hat{\theta}_v - \theta_v^*\| \leq \|\tilde{\theta}_u - \theta_u^*\| + \|\theta_u^* - \theta_v^*\| + \|\hat{\theta}_v - \theta_v^*\|.$$

Therefore,

$$\|\tilde{\theta}_v - \theta_v^*\| \leq \|\tilde{\theta}_v - \hat{\theta}_v\| + \|\hat{\theta}_v - \theta_v^*\| \leq \rho_v^{b_v} (\|\tilde{\theta}_u - \theta_u^*\| + \|\theta_u^* - \theta_v^*\| + \|\hat{\theta}_v - \theta_v^*\|) + \|\hat{\theta}_v - \theta_v^*\|.$$

Taking expectations and using $\mathbb{E}[\|\hat{\theta}_v - \theta_v^*\|] \leq \sigma_v \|\mathbf{A}_v\|_F$ gives

$$\mathbb{E}[\|\tilde{\theta}_v - \theta_v^*\|] \leq \rho_v^{b_v} \left(\mathbb{E}[\|\tilde{\theta}_u - \theta_u^*\|] + \|\theta_u^* - \theta_v^*\| \right) + \sigma_v (1 + \rho_v^{b_v}) \|\mathbf{A}_v\|_F,$$

as claimed. \square

Expected path-wise propagation. By the expected noisy edge-wise propagation lemma, for each $i \geq 1$,

$$\mathbb{E}[\|\tilde{\theta}_{v_i} - \theta_{v_i}^*\|] \leq \rho_{v_i}^{b_{v_i}} (\mathbb{E}[\|\tilde{\theta}_{v_{i-1}} - \theta_{v_{i-1}}^*\|] + \|\theta_{v_{i-1}}^* - \theta_{v_i}^*\|) + \sigma_{v_i} (1 + \rho_{v_i}^{b_{v_i}}) \|\mathbf{A}_{v_i}\|_F.$$

Applying this inequality to v_1 yields

$$\mathbb{E}[\|\tilde{\theta}_{v_1} - \theta_{v_1}^*\|] \leq \rho_{v_1}^{b_{v_1}} \left(\mathbb{E}[\|\tilde{\theta}_{v_0} - \theta_{v_0}^*\|] + \|\theta_{v_0}^* - \theta_{v_1}^*\| \right) + \sigma_{v_1} (1 + \rho_{v_1}^{b_{v_1}}) \|\mathbf{A}_{v_1}\|_F.$$

Applying the same inequality to v_2 and bounding the expectation term,

$$\begin{aligned} \mathbb{E}[\|\tilde{\theta}_{v_2} - \theta_{v_2}^*\|] &\leq \rho_{v_2}^{b_{v_2}} \rho_{v_1}^{b_{v_1}} \mathbb{E}[\|\tilde{\theta}_{v_0} - \theta_{v_0}^*\|] + \rho_{v_2}^{b_{v_2}} \rho_{v_1}^{b_{v_1}} \|\theta_s^* - \theta_{v_1}^*\| + \rho_{v_2}^{b_{v_2}} \|\theta_{v_1}^* - \theta_{v_2}^*\| + \rho_{v_2}^{b_{v_2}} \sigma_{v_1} (1 + \rho_{v_1}^{b_{v_1}}) \|\mathbf{A}_{v_1}\|_F \\ &\quad + \sigma_{v_2} (1 + \rho_{v_2}^{b_{v_2}}) \|\mathbf{A}_{v_2}\|_F. \end{aligned}$$

Proceeding inductively, each step multiplies all upstream terms by $\rho_{v_i}^{b_{v_i}}$ and adds a new distance term discounted by downstream contractions, together with a new noise contribution discounted only by refinements performed after node v_i . Collecting terms yields

$$\mathbb{E}[\|\tilde{\boldsymbol{\theta}}_v - \boldsymbol{\theta}_v^*\|] \leq P_{1:m}\mathbb{E}[\|\tilde{\boldsymbol{\theta}}_{v_0} - \boldsymbol{\theta}_{v_0}^*\|] + \sum_{i=1}^m P_{i:m}\|\boldsymbol{\theta}_{v_{i-1}}^* - \boldsymbol{\theta}_{v_i}^*\| + \sum_{i=1}^m P_{i+1:m}\sigma_{v_i}(1 + \rho_{v_i}^{b_{v_i}})\|\mathbf{A}_{v_i}\|_F,$$

with the convention that empty products equal 1. This concludes the proof. \square

C. Distance metrics for MST-based cascades

We group the task distance metrics used to construct MST-based cascades into the following families, summarized in Figure 4 according to the type of information they require and the level at which task similarity is assessed. Some of these measures are divergences rather than true metrics, but are used as nonnegative edge weights for MST construction.

- **Feature-based distances.** These distances compare task feature representations $\mathbf{X}_v \in \mathbb{R}^{n \times d}$.
 - *Feature distance.* When feature matrices have identical shape, we use a normalized Euclidean distance between flattened representations

$$d_{\text{feat}}(u, v) = \sqrt{\frac{1}{D} \left\| \text{vec}(\mathbf{X}_u) - \text{vec}(\mathbf{X}_v) \right\|^2},$$

where D is the number of overlapping dimensions. When shapes differ, each task is embedded using concatenated empirical means and variances, and the same normalized Euclidean distance is applied.

- *Maximum Mean Discrepancy (MMD).* Let $\mathbf{X}_u = (\mathbf{x}_{u,1}, \dots, \mathbf{x}_{u,n})^\top$ and $\mathbf{X}_v = (\mathbf{x}_{v,1}, \dots, \mathbf{x}_{v,n})^\top$ denote the feature matrices of tasks u and v . Using an RBF kernel k_σ , we define

$$d_{\text{MMD}}(u, v) = \left\| \mathbb{E}_{\mathbf{x} \sim \hat{P}_u} [\varphi(\mathbf{x})] - \mathbb{E}_{\mathbf{x} \sim \hat{P}_v} [\varphi(\mathbf{x})] \right\|_2,$$

where \hat{P}_u denotes the empirical distribution supported on the rows of \mathbf{X}_u , and φ is a random Fourier feature approximation of k_σ with bandwidth σ selected using the median heuristic.

- *Gaussian mean–covariance distance.* Approximating each feature distribution by a Gaussian $\mathcal{N}(\boldsymbol{\mu}_v, \boldsymbol{\Sigma}_v)$, we define

$$d_{\text{Gauss}}(u, v) = \|\boldsymbol{\mu}_u - \boldsymbol{\mu}_v\| + \|\boldsymbol{\Sigma}_u - \boldsymbol{\Sigma}_v\|_F.$$

- *Centered Kernel Alignment (CKA) distance.* Given centered representations $\mathbf{Z}_u \in \mathbb{R}^{n \times d}$ and $\mathbf{Z}_v \in \mathbb{R}^{n \times d}$, we use linear kernels $\mathbf{K}_u = \mathbf{Z}_u \mathbf{Z}_u^\top$ and $\mathbf{K}_v = \mathbf{Z}_v \mathbf{Z}_v^\top$ and their centered versions $\tilde{\mathbf{K}}_u = \mathbf{H} \mathbf{K}_u \mathbf{H}$, $\tilde{\mathbf{K}}_v = \mathbf{H} \mathbf{K}_v \mathbf{H}$, where $\mathbf{H} = \mathbf{I}_n - \frac{1}{n} \mathbf{1} \mathbf{1}^\top$. We define

$$\text{HSIC}(\mathbf{K}_u, \mathbf{K}_v) = \text{tr}(\tilde{\mathbf{K}}_u \tilde{\mathbf{K}}_v),$$

where HSIC stands for Hilbert-Schmidt Independence Criterion, and define the CKA similarity as

$$\text{CKA}(u, v) = \frac{\text{HSIC}(\mathbf{K}_u, \mathbf{K}_v)}{\sqrt{\text{HSIC}(\mathbf{K}_u, \mathbf{K}_u) \text{HSIC}(\mathbf{K}_v, \mathbf{K}_v)}}.$$

Finally, we set the dissimilarity to $d_{\text{CKA}}(u, v) = 1 - \text{CKA}(u, v)$.

- **Target-based distances.** These distances compare task outputs $\mathbf{y}_v \in \mathbb{R}^n$ directly.

- *Target distance.*

$$d_{\text{target}}(u, v) = \|\mathbf{y}_u - \mathbf{y}_v\|.$$

- *Symmetric Kullback–Leibler (KL) divergence.* Let p_v denote a smoothed empirical histogram of \mathbf{y}_v . We define

$$d_{\text{KL}}(u, v) = \frac{1}{2} (\text{KL}(p_u \| p_v) + \text{KL}(p_v \| p_u)).$$

- Jensen–Shannon distance.

$$d_{\text{JS}}(u, v) = \sqrt{\frac{1}{2}\text{KL}(p_u\|m) + \frac{1}{2}\text{KL}(p_v\|m)}, \quad m = \frac{1}{2}(p_u + p_v).$$

- Wasserstein distance. We use the 1-Wasserstein distance between empirical target distributions \hat{p}_u and \hat{p}_v ,

$$d_{\text{Wass}}(u, v) = W_1(\hat{p}_u, \hat{p}_v).$$

- **Optimization-geometry distances.** These distances are derived from optimization quantities or model parameters.

- Gradient distance. Using gradients at initialization $\mathbf{g}_v = \mathbf{X}_v^\top \mathbf{y}_v$, optionally normalized,

$$d_{\text{grad}}(u, v) = \|\mathbf{g}_u - \mathbf{g}_v\|.$$

- Model distance. Let $\hat{\boldsymbol{\theta}}_v$ denote the ridge-regression solution for task v . We define

$$d_{\text{model}}(u, v) = \|\hat{\boldsymbol{\theta}}_u - \hat{\boldsymbol{\theta}}_v\|.$$

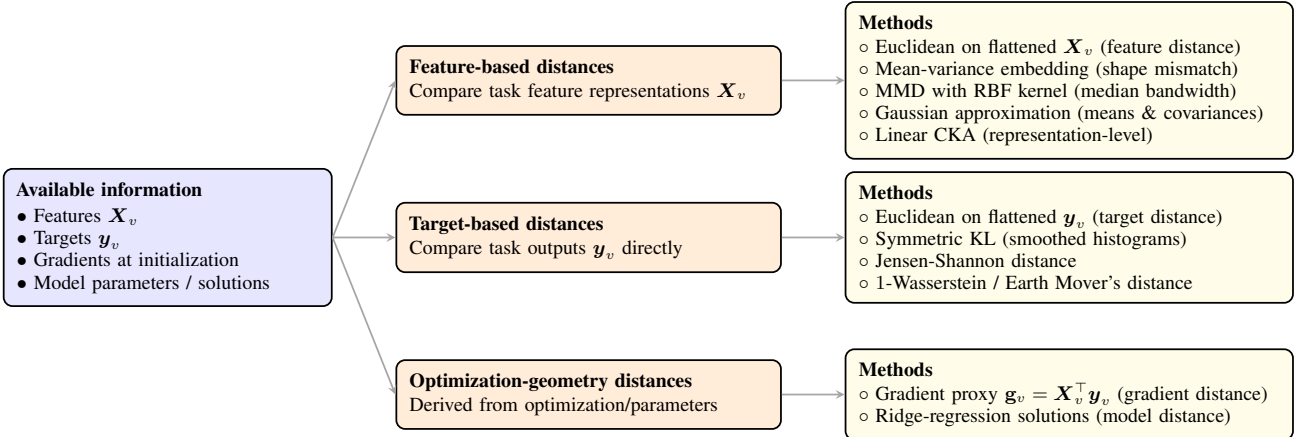


Figure 4. Distance taxonomy for MST-based cascade construction.

While no single measure dominates across all regimes, our results suggest the following heuristics. When labels and optimization information are available, distances derived from gradients or empirical solutions tend to be the most stable, as they align closely with transfer bias. When tasks share similar input representations but differ in targets, feature-based distances provide a reasonable approximation. Target-based or distributional distances are most effective when outputs are low-dimensional and comparably scaled. In highly heterogeneous settings, distances that emphasize locality and avoid long-range connections are preferable regardless of their specific construction.

D. Additional Experimental Results

This section provides complementary visualizations and detailed numerical results that support the main experimental findings. We report extended results for the synthetic regression benchmark and the UK electricity forecasting task experiments.

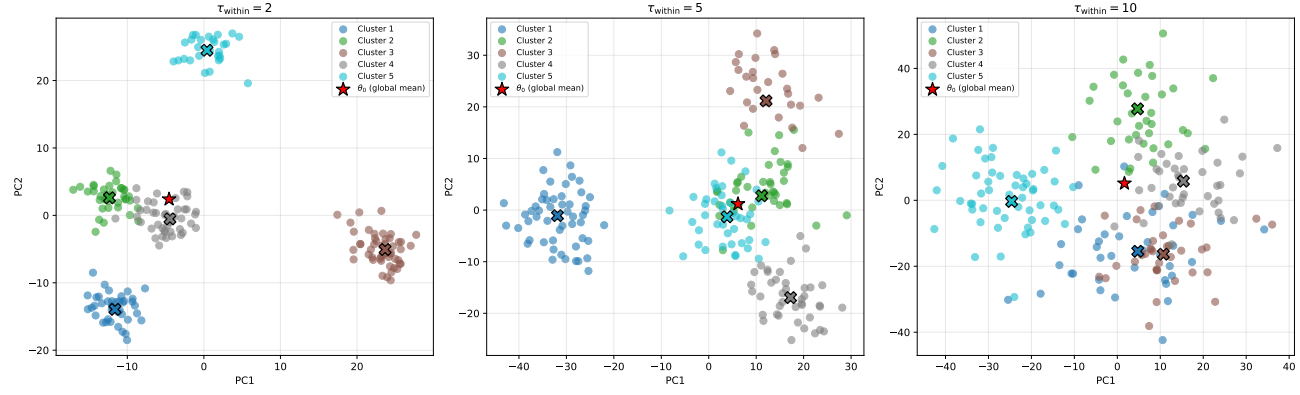
D.1. Synthetic Regression

Figure 5 illustrates the geometry of the synthetic tasks. Increasing the within-cluster variance τ_{within} progressively disperses task parameters while preserving the same between-cluster separation, resulting in a controlled degradation of task similarity.

Figure 6 provides a visual summary of the same sweep, highlighting the relative performance of cascaded transfer strategies across regimes.

Table 3. Unified experimental results across all datasets, for different number of tasks T and global budget B . **Synthetic regression:** Test RMSE. **UK electricity:** Test RMSE (kWh). **Image classification:** Accuracy (%). Each configuration is evaluated across 50 simulations. **Bold** and underlined entries denote best and second-best performance *within each row*.

Dataset	Params	T	B	Indiv	Baselines		Feature	Target	Gradient	Model	CTL-MST variants			MeanCov	JS	CKA
					Star	CTL-RandTree					KL	Wasserstein	MMD			
Synthetic Regression (RMSE)																
Syn-2	200	500	494.2 ± 149.7	440.4 ± 155.9	455.4 ± 192.2	447.9 ± 166.1	445.5 ± 169.1	432.4 ± 153.3	407.7 ± 143.3	440.3 ± 154.3	453.7 ± 156.4	<u>417.4 ± 130.1</u>	460.8 ± 197.7	485.6 ± 254.9	458.4 ± 203.1	
Syn-2	200	1000	458.9 ± 134.2	382.0 ± 139.1	386.1 ± 146.5	363.2 ± 131.7	373.3 ± 121.2	368.8 ± 143.3	356.9 ± 151.3	369.5 ± 132.6	412.8 ± 150.7	400.5 ± 156.9	355.6 ± 130.9	382.7 ± 114.6	385.5 ± 171.9	
Syn-2	200	2000	499.2 ± 178.4	451.6 ± 181.9	409.8 ± 162.5	448.9 ± 187.7	418.4 ± 152.5	370.1 ± 163.8	347.6 ± 144.2	421.5 ± 181.3	428.3 ± 181.5	429.0 ± 191.7	457.6 ± 215.2	403.9 ± 167.0		
Syn-5	200	500	595.9 ± 166.3	547.8 ± 224.6	549.4 ± 164.9	528.9 ± 209.7	522.1 ± 174.2	525.7 ± 176.0	530.0 ± 165.3	543.5 ± 198.8	530.4 ± 173.5	546.5 ± 181.0	537.9 ± 180.4	546.0 ± 171.0	547.8 ± 187.3	
Syn-5	200	1000	550.6 ± 130.7	434.7 ± 142.6	460.1 ± 136.7	449.8 ± 149.6	450.7 ± 150.6	444.5 ± 150.6	460.4 ± 154.9	472.3 ± 164.9	476.2 ± 151.7	466.9 ± 144.3	437.3 ± 149.5	472.9 ± 173.6		
Syn-5	200	2000	590.5 ± 185.7	541.2 ± 187.1	520.6 ± 204.2	517.9 ± 182.0	437.4 ± 152.5	447.1 ± 148.3	511.0 ± 176.4	517.7 ± 184.0	543.5 ± 213.1	517.3 ± 194.4	517.3 ± 184.0	545.2 ± 199.5		
Syn-10	200	500	913.8 ± 168.4	845.5 ± 178.8	872.5 ± 253.1	835.9 ± 189.5	857.8 ± 215.5	844.7 ± 254.5	805.2 ± 187.8	891.9 ± 262.6	860.7 ± 257.7	823.8 ± 227.4	855.7 ± 226.6	800.4 ± 175.3	845.9 ± 213.5	
Syn-10	200	1000	871.5 ± 141.6	802.4 ± 189.5	749.2 ± 171.0	740.1 ± 200.7	768.8 ± 189.2	675.2 ± 152.7	765.2 ± 186.3	749.1 ± 154.2	760.8 ± 195.9	753.8 ± 178.2	747.8 ± 172.4	752.1 ± 178.2		
Syn-10	200	2000	912.8 ± 174.3	930.2 ± 262.4	887.2 ± 246.1	830.6 ± 218.4	814.4 ± 200.9	722.4 ± 175.8	707.2 ± 180.1	808.1 ± 218.3	823.9 ± 243.2	863.1 ± 222.9	858.5 ± 239.2	790.2 ± 220.9	832.2 ± 231.4	
UK Electricity Forecasting (RMSE, kWh)																
UK	100	500	2729.4 ± 8.8	2247.9 ± 51.8	2395.9 ± 59.4	2420.9 ± 45.3	2156.2 ± 51.8	1990.6 ± 41.8	2089.7 ± 42.2	2042.8 ± 52.1	2032.3 ± 48.6	2359.4 ± 54.3	2425.8 ± 55.9	2113.3 ± 43.1	2356.5 ± 46.9	
UK	100	1000	2694.4 ± 9.5	1820.7 ± 38.7	2042.4 ± 36.4	1973.4 ± 39.3	1749.8 ± 29.8	1634.5 ± 22.9	1715.5 ± 29.4	1709.2 ± 27.4	1623.2 ± 21.8	2032.1 ± 37.8	1976.7 ± 34.4	1698.6 ± 26.6	1989.9 ± 39.3	
UK	100	2000	2612.8 ± 7.3	1504.1 ± 19.0	1612.4 ± 16.3	1604.8 ± 16.9	1412.9 ± 10.0	1354.9 ± 6.8	1395.9 ± 7.9	1377.1 ± 6.9	<u>1363.1 ± 6.1</u>	1583.4 ± 18.9	1620.7 ± 19.5	1398.2 ± 10.7	1637.9 ± 19.4	
Image Classification (Accuracy, %)																
FMNIST	200	500	90.6 ± 5.2	90.5 ± 5.2	91.5 ± 4.1	93.5 ± 3.6	91.8 ± 4.0	94.5 ± 3.4	91.1 ± 5.0	89.9 ± 5.2	94.1 ± 3.6	94.7 ± 3.2	89.9 ± 5.2	92.0 ± 4.0		
FMNIST	200	2000	94.5 ± 3.0	94.4 ± 3.3	94.1 ± 3.2	95.1 ± 3.0	94.2 ± 3.0	95.7 ± 2.8	94.4 ± 3.3	94.0 ± 3.9	95.2 ± 3.5	95.8 ± 2.8	94.0 ± 3.9	94.2 ± 3.2		
CIFAR	200	500	60.9 ± 4.7	64.0 ± 4.3	65.2 ± 3.9	65.5 ± 3.8	65.4 ± 3.8	67.7 ± 3.7	65.4 ± 3.6	64.6 ± 3.8	64.6 ± 3.8	65.5 ± 3.4	67.5 ± 4.0	64.6 ± 3.8	65.4 ± 3.9	
CIFAR	200	2000	67.7 ± 3.9	66.7 ± 3.8	67.3 ± 3.5	67.4 ± 3.7	67.3 ± 3.4	69.7 ± 3.7	67.5 ± 3.6	67.0 ± 4.1	67.0 ± 4.1	67.7 ± 3.7	69.1 ± 3.6	67.0 ± 4.1	67.5 ± 3.5	

 Synthetic Tasks ($T=200$, $K=5$, $\tau_{\text{between}} = 10$, $\sigma = 10$)

 Figure 5. Two-dimensional PCA projection of task parameters for the synthetic data with increasing within-cluster variance τ_{within} .

D.2. UK Electricity Forecasting

Figure 7 provides additional context on the UK electricity benchmark. The spatial distribution of the 100 sampled smart meters shows broad geographic coverage, while the consumption histogram highlights a strongly skewed demand distribution with a heavy right tail.

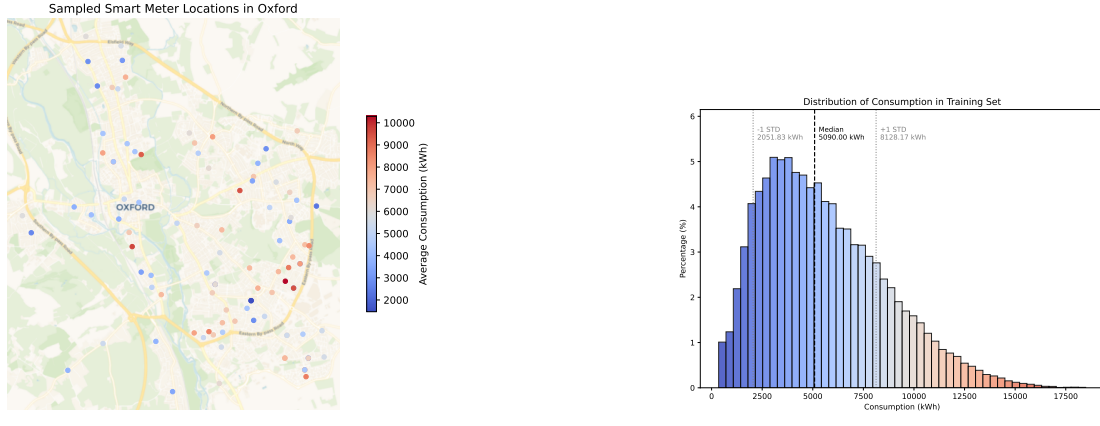


Figure 7. Overview of spatial positions and consumption distribution of the sampled smart meters in Oxford's urban area.

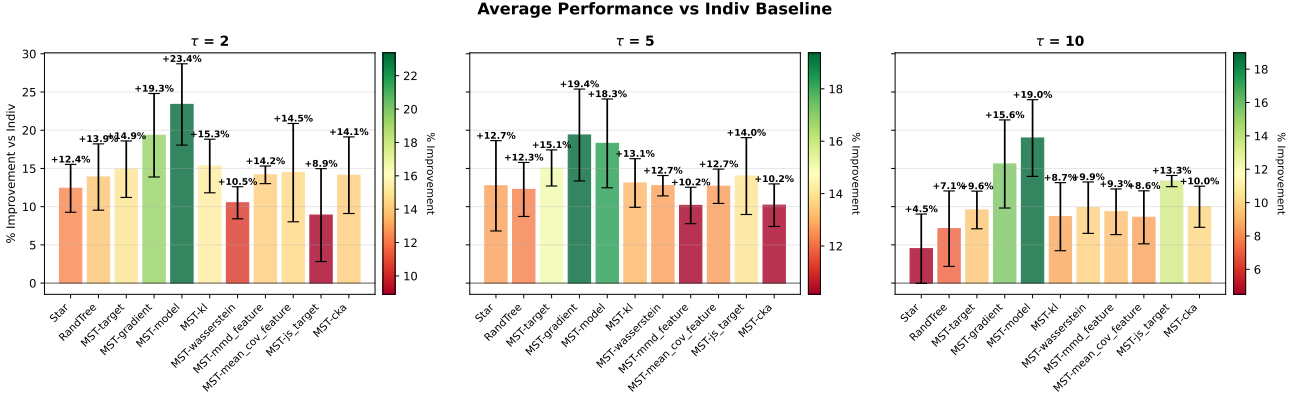


Figure 6. Test RMSE for synthetic tasks across within-cluster variability τ , number of tasks T , and global budgets B .

E. Budget Allocation Ablation Study

This section investigates the impact of the *budget allocation strategy* in CTL. While all main experiments use a uniform allocation of the global budget across tasks, the theoretical analysis in Section 3 suggests that allocating more refinement effort to certain tasks (e.g., deeper nodes in the cascade or tasks connected by longer edges) may further improve performance. We empirically evaluate this question in a controlled synthetic setting.

CTL configuration. We evaluate CTL with minimum spanning tree construction using the gradient-based distance. The seed task is selected using the same procedure as in the main experiments, and the cascade is oriented away from the seed. Models are linear regressors trained by gradient descent. The global budget B is measured in gradient steps and is varied over $B \in \{500, 1000, 2000\}$. A fixed fraction (10%) of the budget is allocated to the seed task, and the remaining budget is distributed across non-root tasks according to the allocation scheme under consideration. Each task is refined exactly once.

Budget allocation schemes. Let $\text{depth}(v)$ denote the depth of node v in the cascade tree, and let $d(u, v)$ denote the edge length between a task and its parent. We compare the following allocation strategies:

- **Uniform:** all non-root tasks receive equal budget.
- **Depth-increasing:** $b_v \propto (\text{depth}(v) + 1)^\alpha$, allocating more budget to deeper tasks.
- **Depth-decreasing:** $b_v \propto (\text{depth}(v) + 1)^{-\alpha}$, favoring tasks closer to the root.
- **Edge-length-based:** $b_v \propto (d(\text{pa}(v), v) + \varepsilon)^\beta$, allocating more budget to tasks whose transfer edge is longer.

We consider $\alpha \in \{1, 2\}$ and $\beta \in \{1, 2\}$. In all cases, real-valued allocations are converted to integer budgets using a largest-remainder scheme, ensuring that $\sum_v b_v = B$ exactly.

Evaluation protocol. For each combination of $(\tau_{\text{within}}, B)$ and allocation scheme, we repeat the experiment over 50 independent random draws of task parameters and data. Performance is measured by the RMSE, averaged across tasks. We report mean and standard deviation over repetitions. Identical trees, seeds, learning rates, and optimization procedures are used across all allocation schemes to ensure a fair comparison.

Results. Figure 8 reports the effect of different budget allocation strategies for CTL-MST-gradient across increasing task heterogeneity $\tau_{\text{within}} \in \{2, 5, 10\}$ and total budgets $B \in \{500, 1000, 2000\}$. Across all regimes, uniform allocation provides a strong and reliable baseline and is never severely suboptimal. In low and moderate heterogeneity settings, uniform allocation often lies within one standard deviation of the best-performing method, particularly at larger budgets, indicating that CTL is not overly sensitive to the precise allocation rule.

At smaller budgets, structure-aware allocations become more influential. In several low-heterogeneity configurations, edge-length-based allocation achieves the lowest RMSE, suggesting that allocating additional refinement steps to tasks connected by longer transfer edges helps mitigate transfer bias when optimization resources are scarce. Depth-increasing

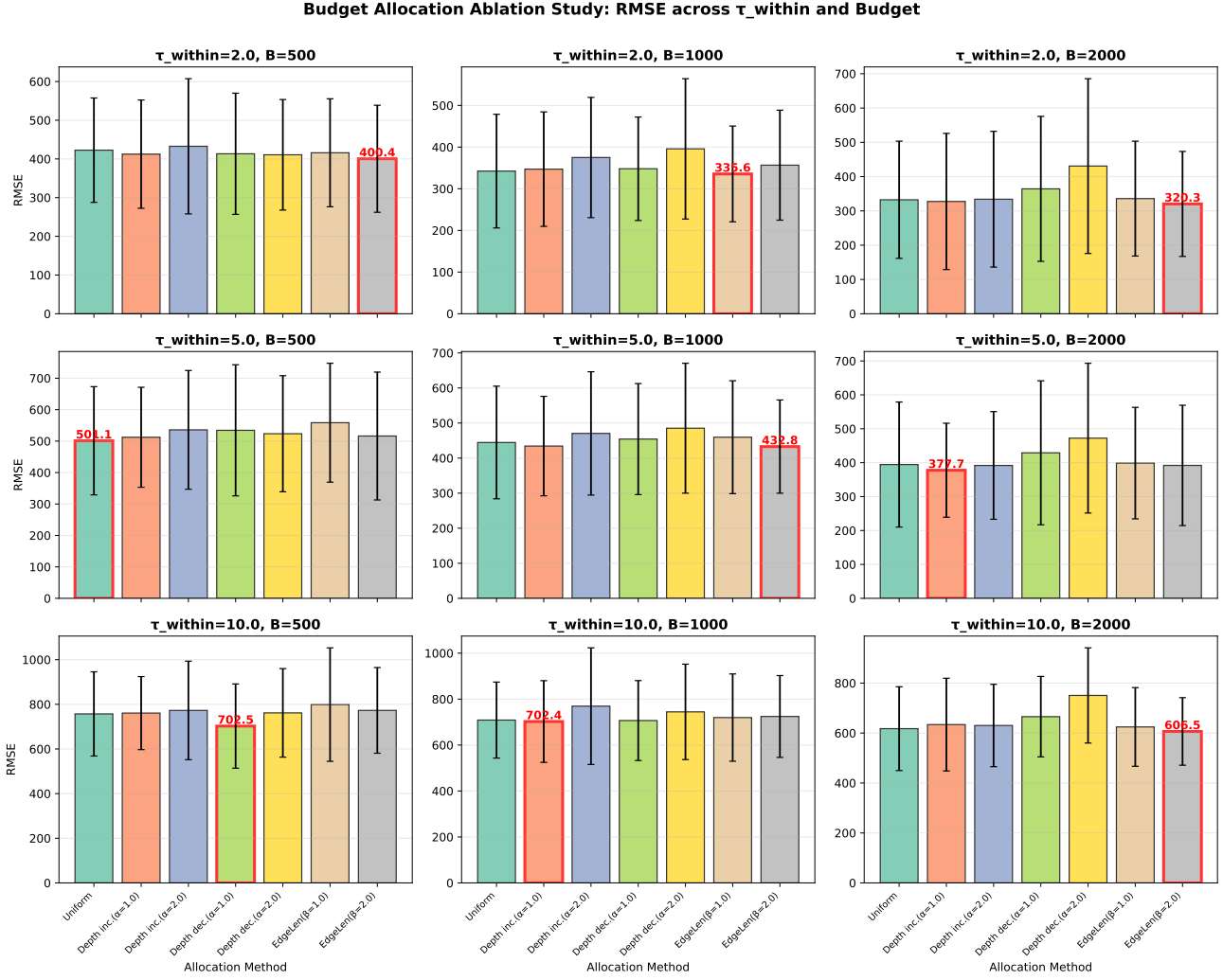


Figure 8. Budget allocation ablation for CTL-MST-gradient on clustered synthetic regression tasks. Each subplot shows mean test RMSE (\pm one standard deviation over 50 runs) for a given τ_{within} and total budget B . Bars correspond to different budget allocation schemes, with the best-performing method highlighted.

allocations occasionally improve performance at intermediate budgets by compensating for accumulated upstream error at deeper nodes, whereas depth-decreasing allocations generally underperform as task heterogeneity increases, indicating that prioritizing early tasks alone is insufficient.

In the high-heterogeneity regime ($\tau_{\text{within}} = 10$), performance differences between allocation schemes narrow and variance increases. While certain structure-aware schemes still achieve the best average RMSE in individual configurations, gains over uniform allocation remain modest, suggesting that budget reallocation cannot fully compensate for weak task relatedness.

Overall, these results support uniform allocation as a robust default, while confirming that simple structure-aware schemes can provide additional gains at no extra computational cost in low-budget and low-to-moderate heterogeneity regimes, in agreement with the theoretical analysis.